INTERNATIONAL JOURNAL FOR NUMERICAL METHODS IN FLUIDS, VOL. 15, 883–894 (1992)

INFLUENCE OF TRAILING-EDGE GRID STRUCTURE ON NAVIER–STOKES COMPUTATION OF TURBOMACHINERY CASCADE FLOW

HEE-TAEG CHUNG* AND JE-HYUN BAEK†

Department of Mechanical Engineering, Pohang Institute of Science and Technology, P.O. Box 125, Pohang, 790-600, Republic of Korea

SUMMARY

Three kinds of grid system based on C-type grid are examined in order to reveal their relative flow characteristics of the turbomachinery cascade, especially near the trailing edge and wake. Here, a semi-conservative interpolation technique to treat the discontinuous boundary condition along the periodic boundary is proposed and is applied on the patched-type grid structure. Computational results are presented to see the influence of trailing-edge grid structure on the Navier–Stokes solutions for the high-turning transonic turbine cascade.

KEY WORDS Trailing-edge grid structure Cubic interpolation technique Implicit LU factorization scheme Transonic turbine cascade

1. INTRODUCTION

Numerical simulation of viscous compressible flow in turbomachinery cascade involves many problems due to the complex geometry of blade but also physical flow phenomena. In general, three different types of grid system have been utilized for the analysis of the cascade flow. These are the O-grid (polar-co-ordinate configuration), the C-grid (parabolic-co-ordinate configuration), and the H-grid (Cartesian-co-ordinate configuration). The latter two systems are particularly suitable to viscous flow studies. Specially, the use of C-type grid avoids the singularity as in the H-grid at the leading edge when the blade possesses a thick rounded leading edge. As the stagger angle increases or when the blade possesses a thick rounded trailing edge typical of turbine cascades, due to a large grid skewness and slope discontinuity near the trailing edge, it is difficult to predict the flow phenomena accurately by a conventional grid structure. In order to predict the complex cascade flow precisely, a suitable grid structure which minimizes disadvantages of the basic grid structure should be chosen and be followed by an appropriate boundary-treating algorithm.

In the present study, an attempt will be made to investigate the viscous flow characteristics of the numerical solution with respect to the mesh structure. In addition, a semi-conservative interpolation technique which will run on the zonal-periodic boundary of the patched-type grid

* Graduate Student in Ph.D. Program.
† Associate Professor.

0271–2091/92/200883–12$11.00

Received December 1991
Revised May 1992

structure is proposed. A turbine cascade under the condition of fully turbulent transonic flow is analysed to study the influence of grid structure on the numerical solution for typical turbomachinery cascade configurations.

2. ANALYSIS

2.1. Choice of grid structures

In the present study, three types of grid structure based on C-grid system as shown in Figures 1(a)–1(c) have been examined. The first grid structure (we call it grid I), shown in Figure 1(a), is the conventional type, which is adapted to the main flow but its high skewness on the suction surface and near-wake region causes a lot of trouble in grid generation and increases the numerical errors of flow solutions. Due to these reasons, it is inadequate for the simulation of the viscous flow, especially around the near-wake region. The second structure shown in Figure 1(b) (termed as grid II) has blade-conforming meshes much as an O-grid would have and is nearly orthogonal around the near-wake region. Since meshes are not generated such that it conforms to the wake flow, the numerical prediction of the viscous flow in the wake region could not be satisfactory, especially with a high turning angle of the cascades. To improve the defects of the above grid structures, the patched grid (grid III) was constructed as shown in Figure 1(c) and the semi-implicit algorithm to treat the discontinuous boundary using the cubic interpolation technique is proposed. This grid structure is orthogonal to the wake centreline as well as to the blade surface and provides a good resolution not only near the blade surface but also in the wake, which is consistent with the boundary layer theory.

2.2. Treatment of periodic boundary condition

In the analysis of the flow through turbomachineries, the boundaries of the computational flow domain can be classified as inflow and outflow boundaries, impermeable solid-wall boundary on the blade surface, and periodic boundaries. Among them, the periodic boundaries are strongly associated with the generation of the computational grid and their treatment affects the numerical solutions. In grid II, which is not highly skewed, a co-ordinate line emanating from a particular point on the lower boundary is attached to the corresponding periodic point on the upper boundary, which is termed as '*line-periodic*'; so, it is possible to impose the repeating boundary condition in an implicit manner. With grid I, though it is line-periodic, high skewness and slope discontinuity on the suction surface and near-wake region make it difficult to impose the implicit boundary treatment.

Grid III allows independent grid generation across the periodic lines. This flexibility results in meshes with discontinuous grid lines or grid-line slopes. To treat the discontinuous boundary condition along the periodic boundary, a semi-conservative zonal technique is proposed utilizing the cubic interpolation technique. A detailed description is given below.

Grid points along the zonal boundary are defined in Figure 2 and the relationship is

$$\mathbf{r}(P_0)=\mathbf{r}(I,J)=\mathbf{r}(K+\Delta K,J)=r(k,J)=\mathbf{r}[\xi(k)]=\mathbf{r}[\Delta K(I)]. \tag{1}$$

For $P_0(I, J)$, $\Delta K(I)$ can be found from $\mathbf{r}(b_0)=\mathbf{r}(K, J)$ using one-dimensional cubic interpolation technique as follows

$$\begin{aligned}\mathbf{r}(\xi)&=F_{\mathrm{CI}}[\mathbf{r}(a_0),\mathbf{r}(b_0),\mathbf{r}(c_0),\mathbf{r}(d_0)]\\&=f_{-1}(\xi)\mathbf{r}(a_0)+f_{-1/3}(\xi)\mathbf{r}(b_0)+f_{1/3}(\xi)\mathbf{r}(c_0)+f_1(\xi)\mathbf{r}(d_0),\end{aligned} \tag{2}$$

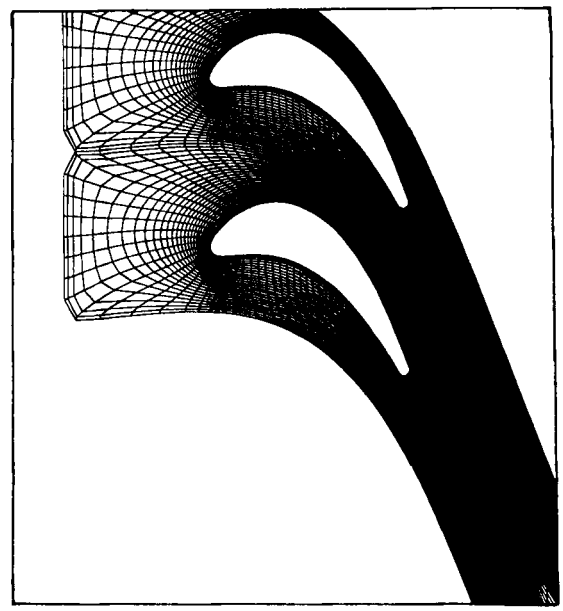

Gloval view

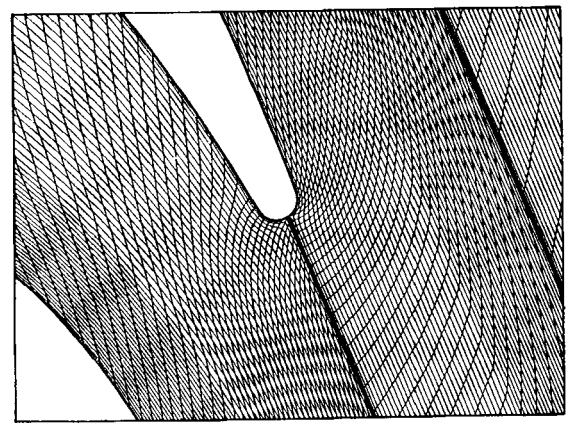

Blow-up near the trailing edge

(a)

Figure 1. Computational grid for VKI transonic turbine cascade flow: (a) grid I; (b) grid II; (c) grid III

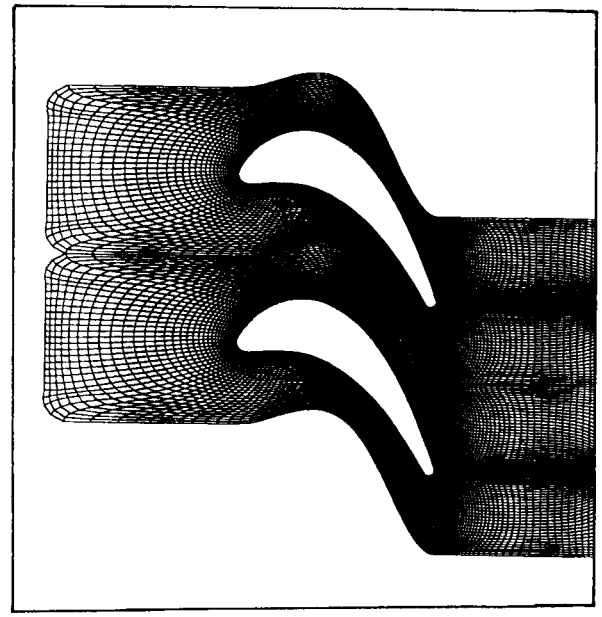

Gloval view

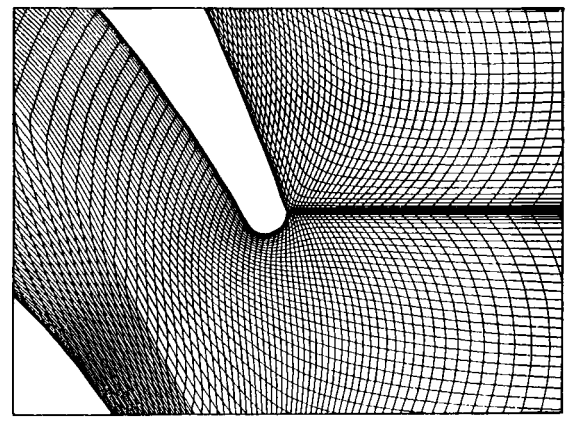

Blow-up near the trailing edge

(b)

Figure 1. (Continued)

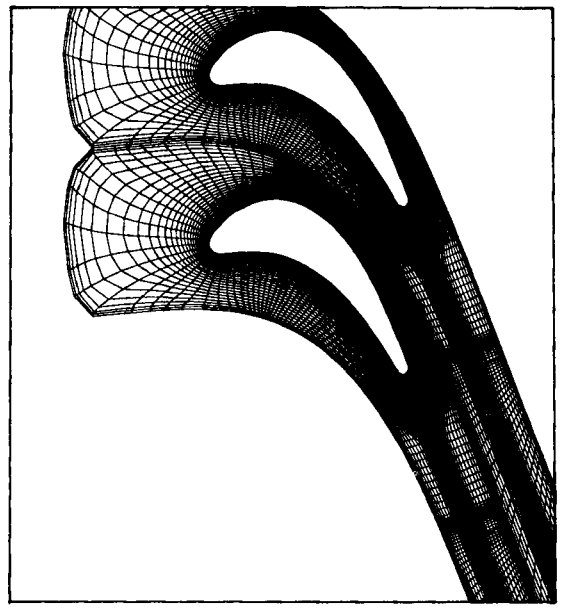

Gloval view

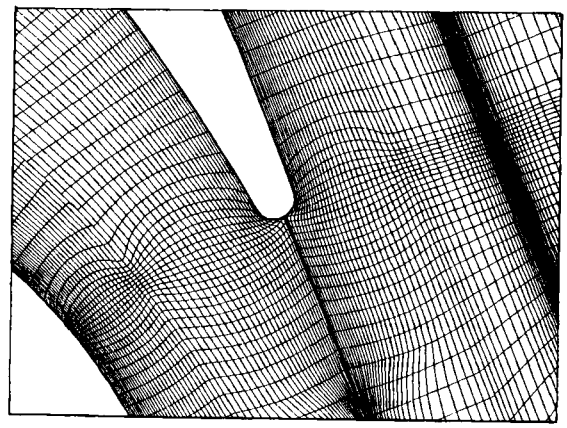

Blow-up near the trailing edge

(c)

Figure 1. (Continued)

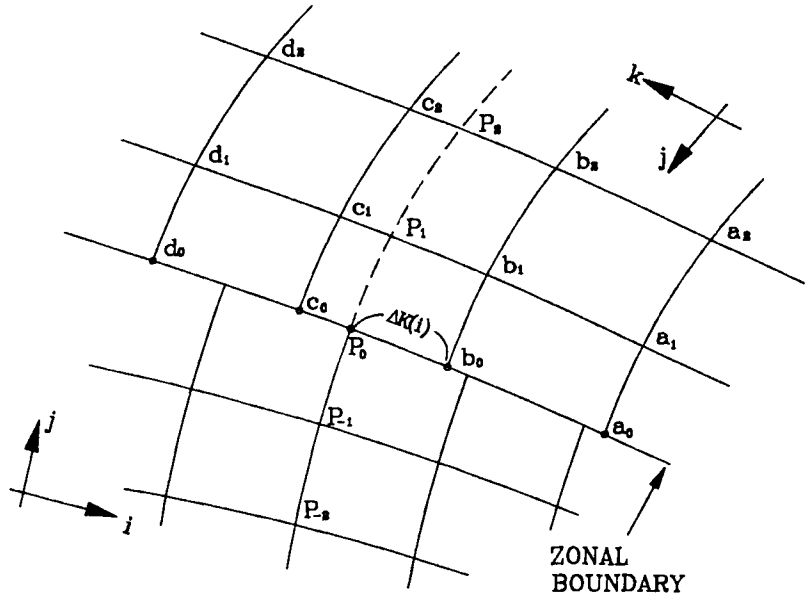

Figure 2. Definition of patched grid structure (grid III) along the periodic boundaries

where

$$\xi = 2/3(k - K - 1/2) \quad \text{and} \quad -1 < \xi < 1,$$

$$f_{-1}(\xi) = 1/16(1-\xi)(9\xi^2 - 1),$$

$$f_{-1/3}(\xi) = 9/16(3\xi - 1)(\xi^2 - 1),$$

$$f_{1/3}(\xi) = -9/16(3\xi + 1)(\xi^2 - 1),$$

$$f_1(\xi) = 1/16(1+\xi)(9\xi^2 - 1).$$

Using $\Delta K(I)$, grid point $\mathbf{r}(P_1)$, $\mathbf{r}(P_2)$ and primitive variables $Q(P_1)$, $Q(P_2)$ in $j = J+1$ and $j = J+2$ can be obtained from equation (2) similarly:

$$\begin{aligned}\varphi(P_1) &= \varphi(I, J+1) = \varphi(K + \Delta K, J+1) = \varphi(\xi_K, J+1) \\ &= F_{\mathrm{CI}}[\varphi(a_1), \varphi(b_1), \varphi(c_1), \varphi(d_1)] \\ &= f_{-1}(\xi_K)\varphi(a_1) + f_{-1/3}(\xi_K)\varphi(b_1) + f_{1/3}(\xi_K)\varphi(c_1) + f_1(\xi_K)\varphi(d_1), \end{aligned} \tag{3}$$

where φ can be primitive flow variables or co-ordinates of grid point.

2.3. *Numerical method*

In the present investigation, the computational method used to solve the Navier–Stokes equations for compressible flow in full conservation form is the finite difference method according to the implicit LU factorization scheme.[1] The numerical methods will be reviewed briefly right after.

The Navier–Stokes equations of the two-dimensional unsteady compressible flow for a generalized co-ordinate system can be written as follows:

$$\hat{U}_\tau + \hat{E}_\xi + \hat{F}_\eta = (\hat{R}_\xi + \hat{S}_\eta)/Re, \tag{4}$$

where $\hat{U}$ represents the conservation variables, $\hat{E}$ and $\hat{F}$ are convective flux vectors and $\hat{R}$ and $\hat{S}$ are the viscous flux vectors. To complete the set of equations, an equation of state for an ideal gas was used for the pressure, and the Baldwin–Lomax algebraic model[2] was applied for the turbulent flow.

The numerical method applied to the governing equations is based on the implicit LU factorization scheme proposed by Obayashi and Kuwahara.[1] In this method, the flux Jacobian matrices which appear in the left-hand side operators in the Beam–Warming method[3] are decomposed into a product of lower and upper bidiagonal matrices by LU factorization, based on the product of flux vector splitting[4] and the implicit MacCormack scheme,[5] in which the simple estimation of eigenvalues of the viscous terms is added. On the other hand, the explicit part is left as in the Beam–Warming method, where central differencing is used. The final form of LU factorization scheme applied to equation (4) is

$$(I+h\nabla_\xi \hat{A}^+ +\varepsilon_i J^{-1}\nabla_\xi J)(I+h\Delta_\xi \hat{A}^- -\varepsilon_i J^{-1}\Delta_\xi J)(I+h\nabla_\eta \hat{B}^+ +\varepsilon_i J^{-1}\nabla_\eta J)$$
$$\times(I+h\Delta_\eta \hat{B}^- -\varepsilon_i J^{-1}\Delta_\eta J)\Delta\hat{U}^n = -h(\delta_\xi(\hat{E}^n-\hat{R}^n/Re)+\delta_\eta(\hat{F}^n-\hat{S}^n/Re))-(D_e|_\xi+D_e|_\eta)J\hat{U}^n, \quad (5)$$

where $D_e|_\xi$ and $D_e|_\eta$ are the dissipative terms, for which an artificial dissipation model having a flux limiter[1] is implemented in the central differencing scheme used here.

The basic algorithm is first-order accurate in time and second-order accurate in space. The scheme requires less computational work and storage since the inversion of the block tridiagonal matrices are reduced to the scalar bidiagonal ones.

3. RESULTS AND DISCUSSION

To investigate the effect of the three basic mesh structures in Figures 1(a)–1(c) on the numerical simulation of the viscous cascade flow and to verify the effectiveness of the boundary treatment technique proposed in Section 2.2, computations were performed for a VKI transonic turbine cascade that has high solidity and is highly cambered. Related experiments were done by Kiock *et al.*[6] in four European wind tunnels. The solidity of this cascade with respect to chord length is 1·41, and the flow conditions for computations are transonic with a high flow turning angle: $M_{in}=0{\cdot}268$, $\beta_{in}=30°$, $M_{ex,is}=1{\cdot}001$ and $\beta_{ex,is}=\cos^{-1}(o/s)=67{\cdot}8°$. Details of the cascade configuration and the flow conditions are described in Reference 6.

The computational meshes of grids I and II are generated using an elliptic grid generating method according to GRAPE algorithm[7] in the entire computational domain. For grid III, an algebraically generated grid at the rear part of the blade and wake field is patched into the upstream region, where the elliptic method was used. This modified C-grid structure, as in Figure 1(c), has been found to reduce the grid skewing in the wake region and much less computational time is required by the Poisson solver compared to the standard C-grid applications [Figures 1(a) and 1(b)] for cascades over a wide range of turning and solidity. This grid structure is orthogonal to the wake centreline as well as to the blade surface and provide a good resolution near the blade surface. Thus, this patched grid provides more flexibility in controlling the meshes for a typical turbomachinery cascade than a standard C-grid does, especially with a large camber and a rounded edge.

Figures 3(a)–3(c) show the computed distribution of Mach number contour in the passage of the cascade. For the transonic flow in a two-dimensional turbine cascade, two weak oblique shocks are generated at the trailing edge; the shock at the suction side is dissipated into the outward wake fields, while the pressure-side shock interacts with the boundary layer of the suction surface of the adjacent cascades, and is then reflected into the downstream passage. The

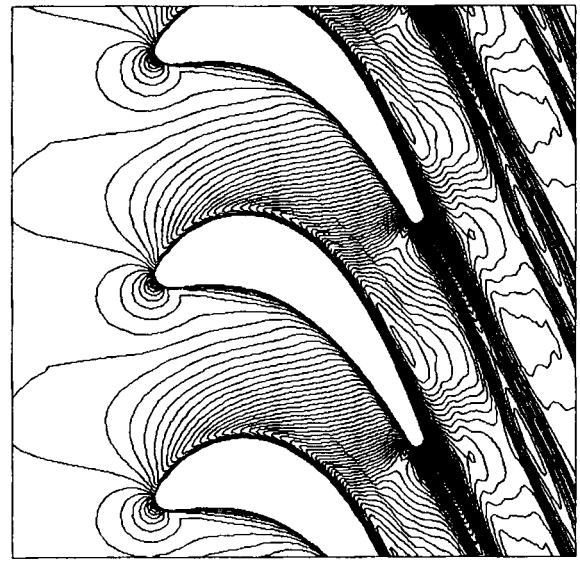

(a)

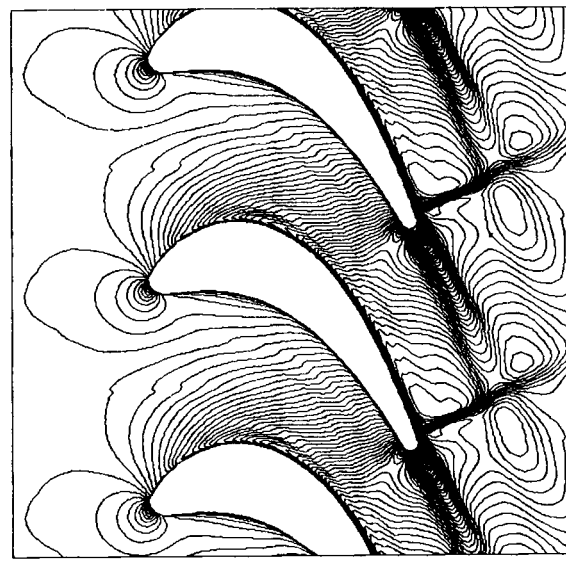

(b)

Figure 3. Mach number contours: (a) by grid I; (b) by grid II; (c) by grid III

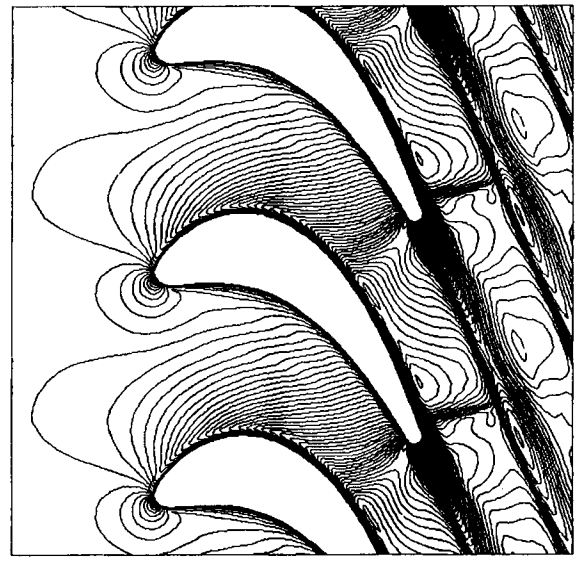

(c)

Figure 3. (Continued)

results of grid I in Figure 3(a) show a qualitative behaviour at the throat of the cascades, but the definite transonic flow pattern cannot be found near the trailing edge. In Figure 3(b), the behaviour of the suction-side shock agrees well with that of the experiments, but the shock interaction with the boundary layer at the throat is not so evident due to the weak shock on the suction surface. Inadequate distribution of mesh points in the wake region causes no pattern of the viscous flow features in the wake boundary layer. Considering the shapes of grids I and II, it can be concluded that the main reason is the high skewness of the mesh system. In Figure 3(c), the behaviour of the suction-side shock agrees well with that of the experiments, and the shock interaction with the boundary layer at the throat is more evident than that of the other grid structures.

The distributions of the computed surface Mach number are shown in Figure 4 together with the experimental results for comparison. From the experimental results, it can be seen that the flow is characterized by acceleration along the suction side up to $X/C=0{\cdot}6$ and followed by moderate deceleration afterwards. Therefore, this deceleration on the suction side from $X/C=0{\cdot}65$ to $0{\cdot}98$ interacts with the shock and may cause separation of the boundary layer flow. It can clearly be seen that only marginal changes occur on the whole pressure side and the suction side up to $X/C=0{\cdot}55$ just before the shock–boundary-layer interaction point. Numerical results of the patched grid (grid III) are seen to agree well with those of the experiments, while those of the other grids (grids I and II) show a little discrepancy on the rear part of the suction, where two peaks of surface Mach number are not found, which implies that numerical diffusion of the standard grid is so strong that the shock behaviour could not be formed on the throat of the passage, as well as in the wake fields. Thus, the patched grid gives a major improvement in the prediction of the complex phenomena at the trailing edge.

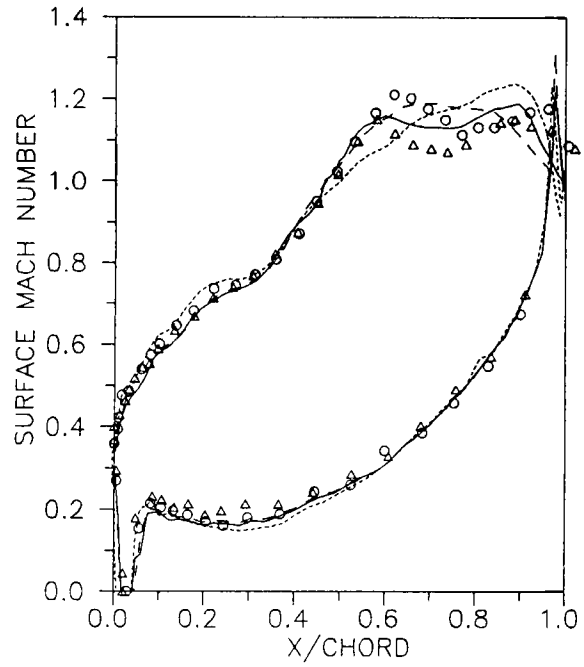

Figure 4. Comparison of surface Mach number distributions. ○ Experiment (OX); △ Experiment (BS);-----grid I; -------grid II;————grid III

In order to be consistent with the boundary layer theory, which is solved along lines perpendicular to the surface, computational grids near the trailing edge are required to be normal to the wake centreline as well as to the blade surface in order to implement the Baldwin–Lomax turbulence model in the present Navier–Stokes scheme. The mesh structure of grid I is not consistent with this constraint due to the high skewness. The body-conforming mesh configuration of grid II is good for flow prediction around the blade surfaces but its independence of the wake flow causes some trouble in applying this computational grid directly to the calculation of the eddy viscosity by the Baldwin–Lomax model. Since the meshes of grid III are generated conforming to the normal co-ordinate system, both on the blade surface and in the wake flow, which are consistent with the boundary layer theory, the eddy viscosity can be computed directly on the computational mesh without having to use an additional grid system for an accurate implementation of the algebraic turbulence model. This increases the accuracy of the turbulence model, particularly in regions of flow where the boundary layer becomes quite thick and allows the model to distinguish where and how the eddy viscosity should decrease away from the wall in the outer layer. Figure 5 shows the variation of the skin friction coefficient on the suction surface. From the result of grid III, transition is seen to occur between 50 and 60% chord, where the shock interacts with the boundary layer on the surface. It is interesting to note that the skin friction of grid I is higher than that of grid III, the reason for which can be induced from the fact that the skewness of grid I causes an overestimation of the normal length scale in turbulence modelling.

The plot of the instantaneous streamlines in Figure 6 shows the flow complexity near the trailing edge of the high cambered turbine cascades, where we can find flow separation, stagnation flow, shock expansion and asymmetric wakes including recirculating bubbles. Not so significant difference with respect to the velocity fields could be found between the three types of

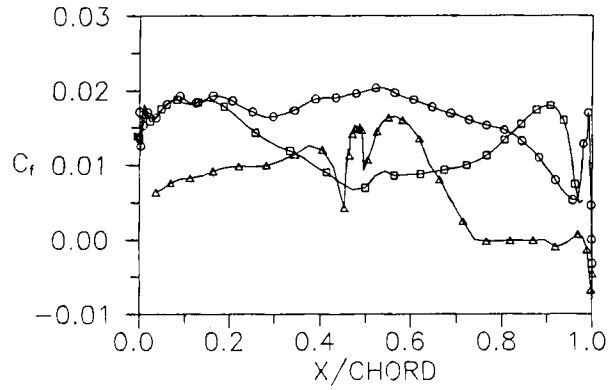

Figure 5. Skin friction coefficient on the blade suction side: —O—O— grid I; —□—□— grid II; —△—△— grid III

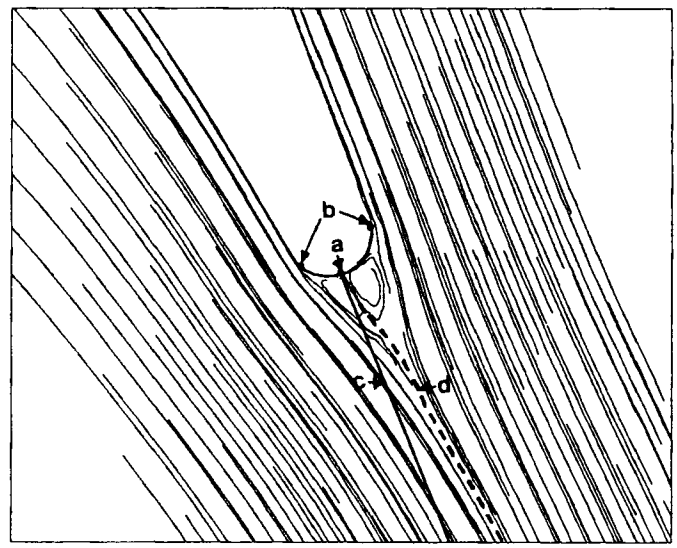

Figure 6. Instantaneous streamline near the trailing edge in turbine cascades: (a) stagnation point; (b) separation point; (c) assumed wakeline; (d) computed wakeline

grid structures. It shows the inadequacy of the present Baldwin–Lomax model for the simulation of the turbulent flow in the near-wake region around a thick rounded trailing edge. The guessed wake centreline used as the branch cut of grids I and III deviates from the actual one, so, the grid is not properly clustered to the shear layer of the wake region. To predict the flow features more precisely near the trailing edge of the cascades, the wakeline-adapted meshes should be used in addition to the physically plausible modelling of turbulent flow by the blade–wake interaction near the trailing edge.

4. CONCLUSIONS

To predict flow fields around the turbomachinery cascade using the Navier–Stokes equations, especially near the trailing edge and wake, three types of grid structure based on C-grid system

are examined with respect to their relative characteristics. Since a semi-conservative zonal technique using a modified cubic interpolation technique coupled with the patched grid structure provides nearly orthogonal grid structure near the trailing edge, it shows good numerical solutions than those of the conventional grid structures. Numerical results of the high-turning transonic turbine cascade flow show the influence of trailing-edge grid structure on the Navier–Stokes solutions through comparisons with the experimental data and the numerical results of each grid structure.

APPENDIX: NOMENCLATURE

$\hat{A}, \hat{B}$	convective Jacobian matrix in the ξ and η directions
$D_e\|_\xi, D_e\|_\eta$	artificial dissipation terms
$\hat{E}, \hat{F}$	inviscid flux vectors in the ξ and η directions
F_{CI}	cubic interpolation function defined in equation (2)
h	time step ($=\Delta t$)
I	identity matrix
J	Jacobian associated with the co-ordinate transformation
M	Mach number
Re	Reynolds number based on the inlet sonic speed
$\mathbf{r}$	position vector ($=x\hat{i}_x+y\hat{i}_y$)
$\hat{R}, \hat{S}$	viscous flux vectors in the ξ and η directions
$\hat{U}$	vector of dependent variables
x, y	Cartesian or physical co-ordinate system

Greek characters

β, β_s	flow angle and blade stagger angle relative to the cascade axis
$\varepsilon_2, \varepsilon_4$	second and fourth-order artificial viscosity coefficient for implicit smoothing
ε_e	artificial viscosity coefficient for explicit smoothing
ξ, η	generalized co-ordinate system
τ	dimensionless time
φ	primitive flow variables or co-ordinates of grid point in equation (3)

REFERENCES

1. S. Obayashi and K. Kuwahara, 'LU factorization of an implicit scheme for the compressible Navier–Stokes equations', *J. Comput. Phys.*, **63**, 157–167 (1986).
2. B. S. Baldwin and H. Lomax, 'Thin-layer approximation and algebraic model for separated turbulent flows', *AIAA Paper 78-257* (1978).
3. R. M. Beam and R. F. Warming, 'An implicit finite-difference algorithm for hyperbolic system in conservation-law forms', *J. Comput. Phys.*, **22**, 87–110 (1976).
4. J. L. Steger and R. F. Warming, 'Flux vector splitting of the inviscid dynamic equations with application to finite-difference methods', *J. Comput. Phys.*, **40**, 263–293 (1981).
5. R. W. MacCormack, 'A numerical method for solving the equations of compressible viscous flow', *AIAA J.*, **20**, 1275–1281 (1982).
6. R. Kiock, F. Lehthaus, N. C. Baines and C. H. Sieverding, 'The transonic flow through a plane turbine cascade as measured in four European wind tunnels', *J. Eng. Gas Turb. Power (Trans. ASME)*, **108**, 277–284 (1986).
7. J. L. Steger and R. L. Sorenson, 'Automatic mesh point clustering near a boundary in grid generation with elliptic differential equation', *J. Comput. Phys.*, **33**, 405–410 (1979).